

## Nature of Current Increase for a CoCrMo Alloy: “transpassive” Dissolution vs. Water Oxidation

Eleonora Bettini\*, Christofer Leygraf, Jinshan Pan

KTH Royal Institute of Technology, School of Chemical Science and Engineering, Department of Chemistry, Div. of Surface and Corrosion Science, Drottning Kristinas väg.51, SE-100 44 Stockholm, Sweden

\*E-mail: [bettini@kth.se](mailto:bettini@kth.se)

Received: 27 June 2013 / Accepted: 29 July 2013 / Published: 10 September 2013

---

The “transpassive” behavior of a CoCrMo alloy has been investigated to clarify the nature of the current increase at high anodic potential (0.5-0.7 V<sub>Ag/AgCl</sub>). The total amount of released metal ions was determined after the potentiostatic measurements. According to the calculation through Faradays’ law, the metal dissolution only contributes to part of the total current recorded. Electrochemical AFM mapping did not show pronounced topography changes at 0.65 V<sub>Ag/AgCl</sub>, while light optical microscopy observation revealed fast evolution of oxygen bubbles. Evidently water oxidation is another important process largely contributing to the current increase at the high potential.

---

**Keywords:** CoCrMo alloy, transpassivity, metal dissolution, water oxidation, AFM

### 1. INTRODUCTION

Nowadays, CoCrMo alloys are widely used in different advance applications under severe service conditions, such as turbines engines [1-2] as well as surgical prosthesis [3-4], due to their high resistance to corrosion and great mechanical properties including slow wear rate. The great corrosion resistance of CoCrMo alloys are related to the spontaneous formation of a protective passive film on the surface, mostly composed of Cr<sub>2</sub>O<sub>3</sub> [5], with minor amount of Co- and Mo-oxides.

Many studies on the corrosion behavior of CoCrMo alloys have been carried out by using electrochemical techniques, such as potentiodynamic polarization, and microscopic analysis by using scanning electron microscopy (SEM) and transmission electron microscopy (TEM), etc [6-13]. Polarization measurements are commonly performed to investigate the corrosion properties of the material, where the experimental conditions may be far from the real application situation. Upon potentiodynamic polarization of the CoCrMo alloy in corrosive electrolytes (e.g., simulated body

fluids) toward high anodic potential, a large increase of the current density is often recorded above the passive potential region in which the current density is very low and almost independent of the potential. However, no clear explanation of the increased current at high anodic potential can be found in literature. In many cases [8-10,13-14], the current increase was interpreted as transpassive dissolution of chromium ( $\text{Cr}^{3+} \rightarrow \text{Cr}^{6+}$ ) because that was observed for pure chromium [15], but without having evidence of the actual occurrence for the CoCrMo alloy. If all the current increase at high potential was given by transpassive dissolution of chromium, the alloy would undergo a fast dissolution and lead to a large amount of  $\text{Cr}^{6+}$  in the solution. Therefore, particular caution in the evaluation and quantification of Cr release must be taken when considering metal dissolution at such accelerated corrosion conditions. For this reason a crucial question is the nature of the observed current increase at high anodic potential, i.e., what are the contributions to the recorded current? The electrochemical instrument just records the total current, which may consist of different contributions given by corrosion reactions as well as redox reactions occurring on the metal surface. Moreover, the corrosion and dissolution behavior of an alloy can be very different from the behavior of a single alloying element, and the microstructure influence on the corrosion behavior must also be taken under consideration. Recently, it was demonstrated by the authors that the microstructure plays an important role in the corrosion resistance of the investigated CoCrMo alloy [16-17]. The matrix areas nearby the micron-sized carbides and the grain boundaries were revealed to be sensitive points for starting of metal dissolution at high anodic potential. The reason was found to be linked to large chromium depletion due to the formation of micron-sized intragranular and nano-sized intergranular carbides.

In this study, efforts were made to elucidate the nature of the current increase at high anodic potential by quantifying the corresponding total metal release and considering the contribution from other anodic reactions. Cyclic potentiodynamic polarization measurements were performed to evaluate the electrochemical behavior of the alloy in phosphate buffer saline (PBS) solution and determine the potential level at which the current density starts to increase drastically. Then, potentiostatic polarization measurements at  $0.7 \text{ V}_{\text{Ag}/\text{AgCl}}$  were performed to record the charge transfer, and the solution was collected for analysis of the amount of metal ions released in the solution by graphite furnace atomic absorption spectroscopy (GF-AAS). A quantitative estimation of the contribution to the total current given by the total metal dissolution at this potential has been made by using the Faradays' law. It may be argued that a polarizing potential up to  $0.7 \text{ V}_{\text{Ag}/\text{AgCl}}$  is unrealistically high for any biomedical application of this alloy. However, it is of principal interest to clarify the nature of the current increase in view of the potential hazards that may arise from an enhanced metal dissolution. In this study just the total metal ions released at high anodic potential has been quantified and no speciation characterization has been performed. Electrochemical reactions that can contribute to the measured current were discussed with respect to the electrode potential and the catalytic properties of the alloying elements. Complementary in situ experiments were performed by using light optical microscopy (LOM) and atomic force microscopy under electrochemical control (EC-AFM) to provide evidence of other possible sources of the current increase.

## 2. EXPERIMENTAL

### 2.1. Material and sample preparation

Samples of a CoCrMo alloy (ASTM F75) were supplied by AB Sandvik Materials Technology, Sweden, in a disc shape of 14 mm in diameter and 2 mm in thickness. The main elemental composition, obtained by optical emission spectroscopy is 28.8 wt.% Cr, 5.4 wt.% Mo, 0.4 wt.% Mn, 0.2 wt.% Ni, 0.2 wt.% Fe, 0.2 wt.% C, bal. Co.

The material tested was cast, then processed by hot isostatic pressing (1200 °C, 103 MPa, 4 hours, slow cooling) followed by high temperature treatment (1200 °C, 4 hours, fast cooling below 800 °C) for reducing the number of defects, such as pores and carbides, obtaining a more homogeneous microstructure (cast-HIP-HT). The samples used for the cyclic polarization were wet ground by using SiC paper successively to 1200 grit. A standard procedure, ultrasonic cleaning in ethanol followed by N<sub>2</sub> gas blow drying, was used to remove contaminants from the sample surface. For the combined potentiostatic polarization measurements and solution analysis that require more careful cleaning, the samples in a disc shape of 14 mm in diameter and 7 mm thick were dry ground to 1200 grit in all the surfaces, then cleaned in an ultrasonic bath first in isopropanol for 7 minutes and then in acetone also for 7 minutes. The samples were then dried by using N<sub>2</sub> gas blowing and stored in a desiccator for at least 24 hours before the measurement. For the in-situ EC-AFM study, the sample was cut from a received disc and mounted on a brass disc by conductive glue. It was then fixed in a plastic mold by epoxy, leaving an exposed surface area of 0.2 cm<sup>2</sup>. The sample was wet ground with SiC paper successively to 4000 grit, followed by a final polish with 0.25 μm diamond paste. Before the measurement the sample was cleaned with ethanol and dried with N<sub>2</sub> gas blowing.

### 2.2. Solutions

In order to clarify the nature of the current increase at high anodic potential, similar conditions to those found in literature were adopted [10,18-19]. A phosphate buffered saline (PBS) solution was prepared with the following composition: 8.77 g/L NaCl, 1.28 g/L Na<sub>2</sub>HPO<sub>4</sub>, 1.36 g/L KH<sub>2</sub>PO<sub>4</sub>. The pH was adjusted to ca. 7.4 with 370 μL of 50% NaOH. For in situ EC-AFM and EC-LOM experiments 3 mM H<sub>2</sub>O<sub>2</sub> was added into the PBS (pH = 7.0). H<sub>2</sub>O<sub>2</sub> is an intermediate product of the water decomposition step reaction [20]. In order to slightly accelerate the water oxidation process occurring at high anodic potential and be able to follow the reaction by AFM, this very low amount of H<sub>2</sub>O<sub>2</sub> was added into the PBS solution. In fact, even without the addition of H<sub>2</sub>O<sub>2</sub>, at sufficient high potential the formation of H<sub>2</sub>O<sub>2</sub> would be unavoidable. Analytical grade chemicals and ultrapure water (Milli-Q, 18 MΩ cm) were used for the solution preparation.

### 2.3. Electrochemical instruments and experiments

A Solartron 1286 electrochemical interface and CorrWare/CorrView software were used for the electrochemical polarization experiments and data analysis. Cyclic potentiodynamic polarization

measurements were performed to investigate passivity and eventual transpassivity of the CoCrMo alloy in the aerated PBS at room temperature. Then, combined potentiostatic measurements at a potential of  $0.7 V_{\text{Ag/AgCl}}$  and analysis of the metal ions dissolved into the solution were carried out, to determine the actual contribution of metal dissolution to the total recorded current. A conventional three electrode cell, with the sample as working electrode, an Ag/AgCl electrode saturated with KCl ( $197 \text{ mV vs. SHE}$ ) as reference electrode and a Pt mesh as counter electrode, was used for the electrochemical measurements. For the cyclic potentiodynamic polarization measurement the solution was added in the amount of ca. 500 mL and the sample area exposed to the electrolyte was  $1 \text{ cm}^2$ . First the open circuit potential (OCP) was recorded for 1 hour, and then the potential was swept from  $-0.2 \text{ V vs. OCP}$  towards anodic potentials with a scan rate of  $10 \text{ mV/min}$ . When the potential reached the value  $0.8 V_{\text{Ag/AgCl}}$  the reversed scan started and the potential was swept towards cathodic potentials.

After 1 hour at OCP condition, the potentiostatic polarization measurements of the CoCrMo alloy were performed at  $0.7 V_{\text{Ag/AgCl}}$  at room temperature. This potential was chosen for the explanation of the origin of the recorded current, because at this level of the potentiodynamic polarization the current has already started to increase. In these measurements, the current was recorded continuously for 2 hours, using a conventional three electrode cell similar to the previously described one, but with a liquid volume of 30 mL. The cell had been previously cleaned carefully with three washing cycles of 10%  $\text{HNO}_3$  followed by Milli-Q water, in order to eliminate possible contamination. The sample area exposed to the electrolyte was  $6.15 \text{ cm}^2$ .

#### 2.4. Metal release analysis

The total concentrations of released metals (Co, Cr and Mo) from the CoCrMo alloy after 2 hours polarization at  $0.7 V_{\text{Ag/AgCl}}$  in PBS solution were analyzed by GF-AAS (Perkin Elmer Analyst 800). The measured concentrations are based on three replicate readings for each sample, and calibrated by quality-control samples of known concentration. More details of the procedures have been previously reported [21-22]. All the results are presented after subtraction of the metal concentrations of blank reference sample (solution without CoCrMo alloy sample). The detection limit of the three alloying elements were,  $15 \mu\text{g/L}$  for Co,  $3 \mu\text{g/L}$  for Cr and  $1,2 \mu\text{g/L}$  for Mo.

#### 2.5. In situ EC-AFM measurements

A Quasent Q-Scope 250 SPM with electrochemical package iProbe, supplied by Windsor Scientific Ltd, UK, was used to perform the in situ AFM measurements. The electrochemical cell used was particularly designed for this application. It was a three electrode type cell where the working electrode, the CoCrMo alloy sample, was tightly fixed at the bottom of the cell, an Ag/AgCl electrode saturated with KCl and a platinum sheet were used as reference and counter electrodes, respectively. The total liquid (PBS +  $3 \text{ mM H}_2\text{O}_2$ ) volume added into the cell was equal to 3 mL. The topography was imaged by contact mode operation in liquid. The probes used were ContAl-G silicon AFM probes, purchased from Budget Sensor, with Al reflex coating, with resonant frequency of  $13 \text{ kHz}$  and spring

constant of 0.2 N/m. The AFM instrument was connected to the iProbe package, able to apply a potential to the sample during the scanning of the topography. In this way the topography changes due to different applied potentials could be imaged. The AFM had also an optical microscope equipped with camera positioned on the top of the AFM head, focused on the scan area and nearby region. The in situ AFM measurements were performed in aerated condition at room temperature. The selected surface area, including large carbides, was scanned with a slow scan rate, 1 Hz, in order to obtain higher quality of the images. The acquisition time for every image was ca. 10 min. The potential of the working electrode was controlled by a potentiostat and referred to the reference electrode used. The sample was left at OCP condition for 2 hours before starting the polarization. The topography images were recorded at different potential values, starting from OCP towards more positive potentials in steps of 0.05 V. Each potential value was hold for 20 minutes and two images were recorded at each potential every 10 minutes. Optical images were also recorded by using the camera on top of the AFM, in order to check topography changes in a larger region nearby the scan area.

### 3. RESULTS AND DISCUSSION

#### 3.1. Cyclic polarization

Figure 1 shows a typical polarization curve obtained for the CoCrMo alloy exposed to PBS. As previously reported [16-17], the alloy exhibits a wide passive range, characterized by a low passive current in the order of  $0.2 \mu\text{A}/\text{cm}^2$  at the scan rate of 10 mV/min. At the potential value around 0.5  $\text{V}_{\text{Ag}/\text{AgCl}}$  the current starts to increase rapidly, reaching the value of  $0.1 \text{ mA}/\text{cm}^2$  at the potential of 0.7  $\text{V}_{\text{Ag}/\text{AgCl}}$ .

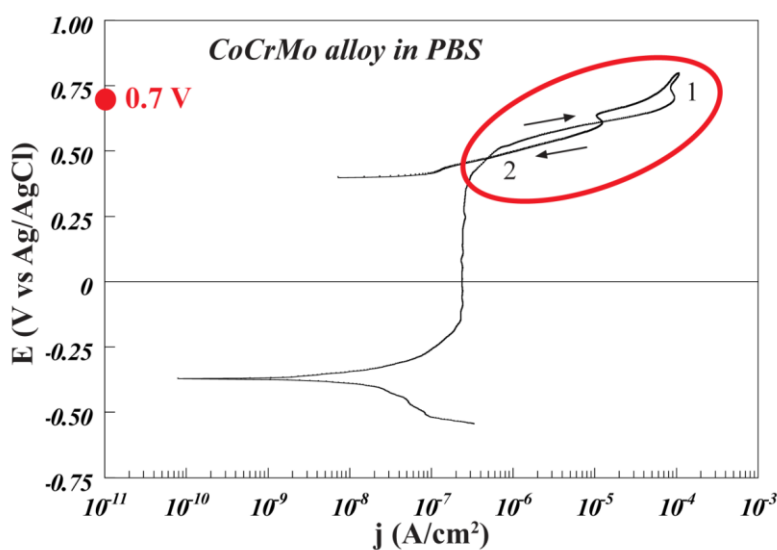
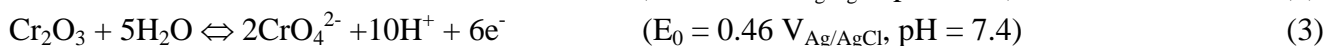
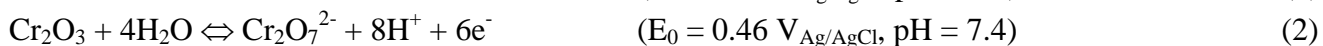
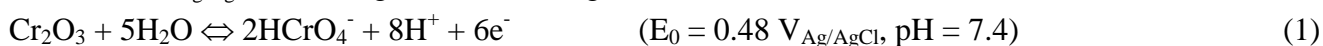


**Figure 1.** Cyclic polarization curve for the CoCrMo alloy in aerated PBS at room temperature (pH = 7.4), scan rate of 10 mV/min, with marked potential value applied to the sample during the potentiostatic polarization measurement followed by metal ions release analyses.

The interpretation of the current increase observed at high anodic potential is not straightforward if the polarization is stopped at a high potential. In order to better understand the dissolution behavior of the alloy a backward potential scan was performed. By comparing the current density recorded during the backward scan to that one recorded during the forward scan at a given potential, one can gain deeper information on the corrosion behavior of the tested material. This has been explained in detail by Pourbaix [23]. If the current density is higher during the backward scan than the forward scan at the same potential, forming a large positive hysteresis loop, this is a clear evidence of occurrence of corrosion at the metal surface, e.g., pitting or crevice corrosion. The opposite situation, a lower current density in the backward scan than the forward scan indicates the absence of corrosion attack, and the current increase is due to other electrochemical reactions taking place on the sample surface.

Two small loops, one negative (loop 1 in Fig. 1) and one positive (loop 2 in Fig. 1), were observed. In the potential range between 0.5 and 0.6  $V_{Ag/AgCl}$ , a small positive hysteresis loop was observed, suggesting that a slight metal dissolution might have occurred at the metal surface. However, above potential 0.6  $V_{Ag/AgCl}$  the small negative loop implies that the electrochemical current density is lower during the backward scan compared to that during the forward scan at the same potential, which suggests that either a protective anodic oxide layer was formed on the sample surface, or some other anodic reactions were slower during the backward scan compared to the forward scan. This is a first indication that most of the current recorded at potential higher than 0.6  $V_{Ag/AgCl}$  is not given by metal dissolution, but due to other redox reactions taking place in the system.

The electrochemical reactions generating the electrochemical current at high anodic potential (above 0.5  $V_{Ag/AgCl}$ ) must be taken into consideration in order to clarify the nature of the current increase recorded at high anodic potential. This large increase of the current density, observed above 0.5  $V_{Ag/AgCl}$ , was previously interpreted by other groups [8-10,13-14], as mostly given by transpassive dissolution of chromium, referring to the behavior of the pure metal. Chromium can be oxidized at around 0.5  $V_{Ag/AgCl}$  according to the following reactions [24]:



However, the thermodynamic predictions from the Pourbaix diagrams are based on pure metals. Cautions must be taken in the interpretation of the corrosion behavior of alloys, which often differ from the pure metals due to the interactions and synergistic effects between the alloying elements. Moreover, other electrochemical reactions taking place on the metal surface must be considered in the discussion of the nature of the recorded current. Depending on the metallic material tested, the species present in the solution and the conditions, other redox reactions, rather than corrosion, can occur at the metal surface, becoming even dominant contributions to the total current recorded by the instrument. In order to obtain quantitative information on the metal release at high potential, potentiostatic measurements at 0.7  $V_{Ag/AgCl}$  for 2 hours were carried out, the PBS solution was collected and the total metal release analyzed.

### 3.2. Potentiostatic polarization

Figure 2 shows an example of a potentiostatic polarization curve of the alloy exposed to PBS at a constant potential of  $0.7 V_{Ag/AgCl}$ . The high current density ( $j$ ) recorded in the very first few seconds is mostly given by the charging of the double layer at the metal-electrolyte interface and, as it can be observed, it decreases rapidly and continuously with time. In fact, it reaches a value of ca.  $20 \mu A/cm^2$  after 2 hours exposure at  $0.7 V_{Ag/AgCl}$ . The decreasing trend of the current density implies that no severe corrosion process is occurring at the sample surface. Figure 2 shows also the integrated charge density ( $Q$ ) vs. time. In this curve, the first region with a higher slope indicates a considerable amount of charge transfer due to a higher current flow, while the second region with a lower slope (lower current density) suggests a decrease of the electrochemical reactions rates, probably due to repassivation of the metal surface. It can be also seen that the high current density in the very first few seconds did not result in a considerable charge transfer due to the very short period.

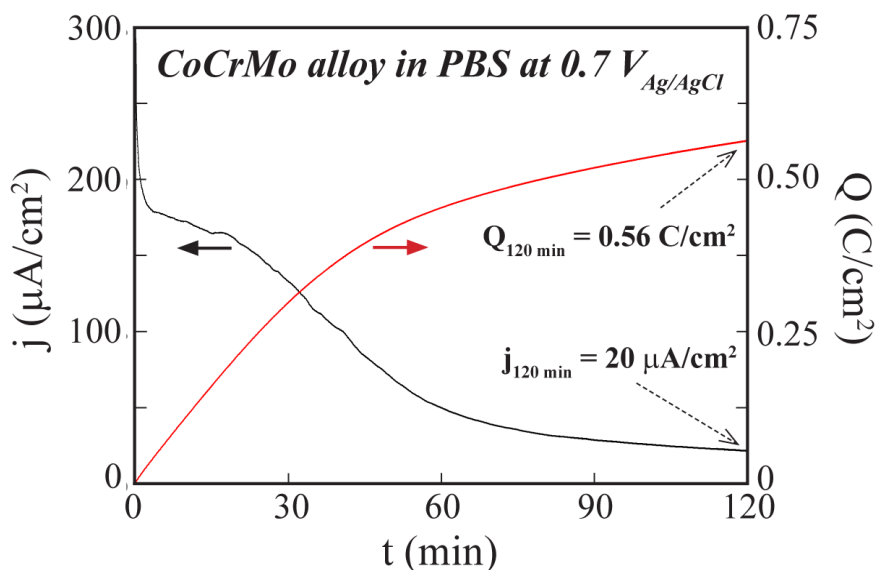


**Figure 2.** Potentiostatic polarization curves for the CoCrMo alloy at  $0.7 V_{Ag/AgCl}$  in PBS at room temperature (pH 7.4), showing the current density ( $j$ ) vs. time and the integrated charge density ( $Q$ ) vs. time. The values of current and charge densities after 2 hours are also shown.

Although some metal dissolution may have occurred during the initial period of exposure at  $0.7 V_{Ag/AgCl}$ , the metal surface was able to regain a passive condition, decelerating the metal dissolution process. A similar behavior has been observed previously for many other corrosion resistant materials, such as ferritic, austenitic and duplex stainless steel [25-26]. The metal release rate was high in the first period of exposure, but decreased continuously later as a result of gradual formation of a more corrosion-resistant surface film during the exposure [26].

Hypothetically, if the high current density recorded at  $0.7 V_{Ag/AgCl}$  was given by transpassive dissolution of the material, the sample surface should have undergone a fast uniform corrosion, like

unprotected carbon steels in an aggressive environment. In contrary, in the previous studies by the authors [16-17], it was shown that at this high anodic potential metal dissolution starts preferentially from the matrix areas adjacent the micron-sized carbides and the grain boundaries, which are precipitation sites of nano-scale carbides. These areas have a higher tendency for metal dissolution because of the chromium depletion [17]. Seyeux et al. [27] demonstrated by using mathematical models that, at high anodic potential, passivity breakdown events occur locally and are preferentially localized at the grain boundaries, due to the lower resistivity of the passive film in these sites. Macdonald [28] in the “Point Defect Model” (PDM) explained that passivity breakdown occurs at the regions of the passive film with high cation vacancy diffusivities. Corrosion initiation is due to the condensation of cation vacancies at the metal/film interface, causing local detachment of the film from the metal [28]. The heterogeneity of the passive film of the CoCrMo alloy caused by the microstructure, especially the presence of carbides and grain boundaries, makes dissolution at high potential to initiate locally at specific weak points [28]. Hence, the transpassive dissolution process is far from being uniform [28].

### 3.3. Metal release analysis

The total amount of alloying elements released during 1 hour exposure at OCP conditions was measured and successively neglected from the following analysis at  $0.7 V_{Ag/AgCl}$  due to the very low concentrations found. Figure 3a and 3b show the quantities ( $\mu\text{g}/\text{cm}^2$ ) and the percentage (wt.%), respectively, of the total metal ions released from the CoCrMo alloy sample after the exposure to PBS for 2 hours at the constant applied potential of  $0.7 V_{Ag/AgCl}$ .

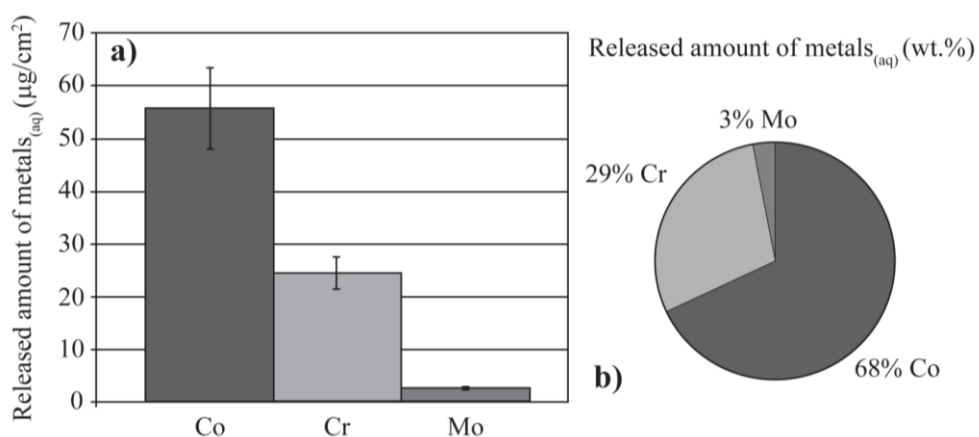


**Figure 3. a-b)** Amount ( $\mu\text{g}/\text{cm}^2$ ) and percentage (wt.%), respectively, of total metal ions for each element (Co, Cr and Mo) released from the CoCrMo alloy exposed in PBS for 2 hours at constant potential of  $0.7 V_{Ag/AgCl}$  at room temperature (pH = 7.4).

The total amount of cobalt detected in the PBS solution was much higher compared to the other two elements, chromium and molybdenum. This was expected since cobalt is the base metal of the

alloy. From the diagram in Figure 3b it can also be observed that the release of the three elements was nearly stoichiometric, with 68% cobalt, 29% chromium and 3% molybdenum released, close to their content in the alloys (64.8% cobalt, 28.8% chromium and 5.4% molybdenum). These results indicate that the metal dissolution at this potential is nearly proportional to the composition of the alloy, rather than dominated by chromium dissolution.

This is contradictory to transpassive dissolution, where uniform dissolution from the entire exposed surface takes place and the amount of released metal ions should be close to the composition of the oxide layer. Milošev et al. [13] studied the change of oxide layer composition at different applied potentials for a CoCrMo alloy of similar composition. It was found that at potentials below  $0.24 V_{Ag/AgCl}$  the passive film consists mainly of  $Cr_2O_3$ . The fraction of CoO in the passive film increases with potential and, in the region from  $0.40$  to  $0.56 V_{Ag/AgCl}$ , the fractions of chromium and cobalt are approximately the same. At potentials higher than  $0.56 V_{Ag/AgCl}$  the content of cobalt decreases again. It was also observed that the content of cobalt is much lower in the surface oxide layer than in the bulk, whereas the contents of chromium and molybdenum in the oxide layer are higher than in the bulk, the former over the whole potential range, and the latter at potentials over  $0.40 V_{Ag/AgCl}$  [13]. In the present study, the amount of alloying elements detected in the solution was found to be close to the bulk alloy composition, which is in accordance with localized dissolution at weak sites, rather than uniform dissolution of the surface oxide layer due to further oxidation of trivalent chromium into soluble chromate species (Eqs. 1-3).

**Table 1.** Total amount of metal ions released for each element detected by GF-AAS after 2 h exposure at  $0.7 V_{Ag/AgCl}$  in PBS. The  $n$  is the metal ion valence used in the calculation and  $Q_{AAS}$  is the charge transferred based on the amount of released metal ions. The released mass and the transferred charge are normalized to the exposed sample area.

Faraday's calculation				
Alloying elements	Metal release ( $\mu\text{g}/\text{cm}^2$ )	$n$	$Q_{AAS}$ ( $\text{C}/\text{cm}^2$ )	Contribution to total current
Co	55.8	1	0.09	16%
Cr	24.3	3	0.13	24%
Mo	2.6	2	0.005	1%

Quantification of the real contribution of metal dissolution to the total current recorded at high anodic potential can be made by measuring the total metal ions released into the solution and calculating the corresponding charge transfer according to the Faradays' law. The amount of charge transfer given by the metal release at  $0.7 V_{Ag/AgCl}$  during 2 hours exposure in PBS can be calculated from the Faradays' law as below (Eq. 4):

$$Q = (\Delta m * n * F) / M \quad (4)$$

where  $Q$  and  $\Delta m$  are the transferred charge ( $C/cm^2$ ) and the released mass ( $g/cm^2$ ), respectively, normalized to the exposed sample area.  $n$  the valency number of ions of the metal element,  $F$  the Faradays' constant ( $96485 C/mol$ ) and  $M$  is the molar mass ( $g/mol$ ).

The transferred charge corresponding to the dissolution of each alloying element has been calculated using the total released mass of each alloying element detected by GF-AAS analysis as input data. Table 1 shows the data from the calculation: the total amount of metal ions released for each element detected by GF-AAS, the ion valences used for calculation, the corresponding transferred charges according to the Faraday's law, and the contribution in percentage to the total current given by the dissolution of the three main alloying elements.

Before the potentiostatic polarization at  $0.7 V_{Ag/AgCl}$ , the CoCrMo alloy was left at OCP condition for 1 hour. For such a highly resistive alloy with spontaneous passivity, it is reasonable to assume that a protective passive layer consisting of stable oxides of the alloying elements had been formed on its surface during this period. Therefore, the further oxidation reactions of the surface oxides upon anodic polarization at  $0.7 V_{Ag/AgCl}$ , i.e., the oxidation state transformations considered in the calculation (Eqs. 5-7), following Pourbaix thermodynamic predictions [24], are:



Based on these considerations, the calculation shows that only ca. 40% of the total current recorded at  $0.7 V_{Ag/AgCl}$  could be given by the total metal dissolution. Moreover, as seen in Fig. 3b, just 29% of the total metal release is due to chromium dissolution. This implies that the high current recorded is not dominated by chromium dissolution. In addition, the X-ray photoelectron spectroscopy (XPS) results obtained by Hodgson et al [9] at high anodic potential, where the current already started to increase, indicated that a thick Cr oxide film was constantly present on the surface, despite the current raise. The experimental results and the calculation suggest that most likely a large part of the current is given by other electrochemical reactions rather than metal dissolution reactions at the oxide present.

### 3.4. In situ EC-AFM monitoring

In order to gain further information on possible sources for the current increase at high anodic potential the topography changes were followed by in situ EC-AFM as a function of the applied potential and time. A  $30 \mu m \times 30 \mu m$  area containing a large carbide and some defects (voids, or part of the carbide pulled off during the grinding and polishing) was selected and maintained in focus for the entire experiment to follow the topography changes at increasing applied potential. Examples of topography images obtained by the in situ EC-AFM are shown in Figure 4.

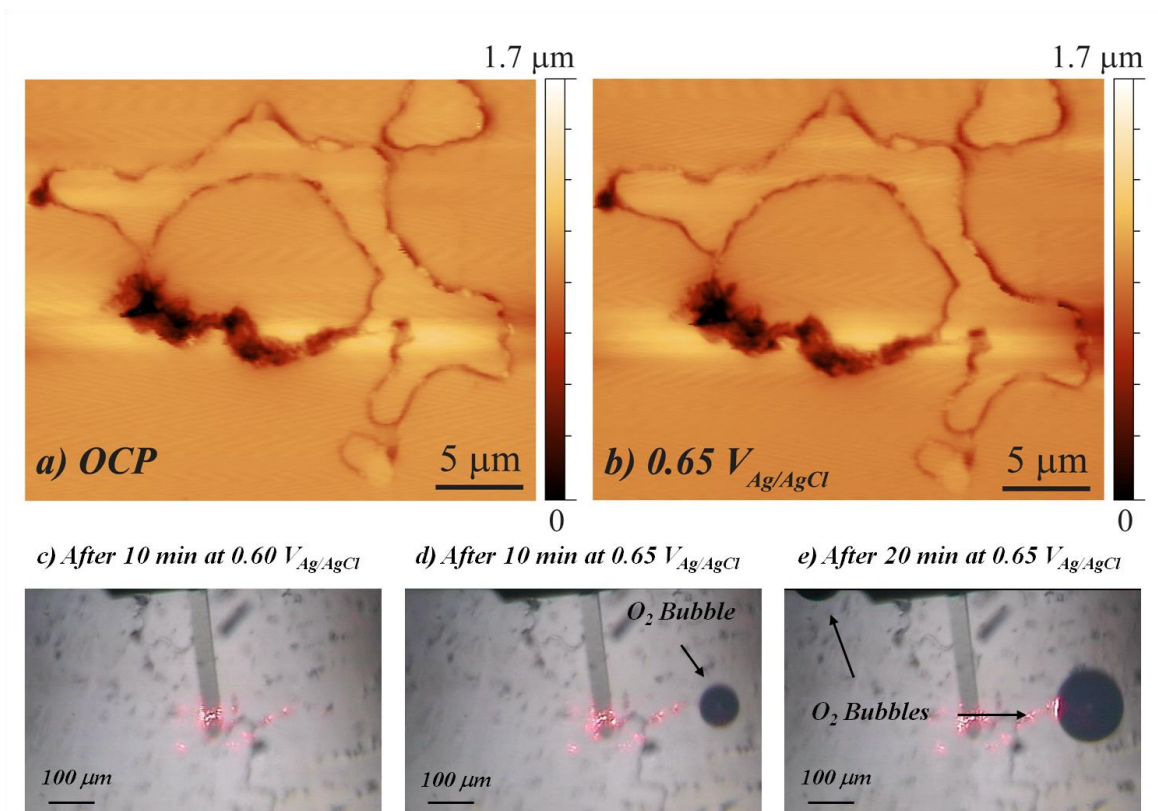


**Figure 4.** a-b) in situ AFM topography images of the same area of the alloy in PBS + 3 mM H<sub>2</sub>O<sub>2</sub> at room temperature (pH = 7.0), after 120 min at OCP and 20 minutes at 0,65 V<sub>Ag/AgCl</sub>, respectively. c-e) Camera monitoring of oxygen bubbles nucleation and growth on the surface, the same area as the AFM imaging. The sample was under potential control in PBS + 3 mM H<sub>2</sub>O<sub>2</sub> (pH = 7.0), after 10 min at 0,60V<sub>Ag/AgCl</sub>, after 10 min at 0,65V<sub>Ag/AgCl</sub>, and after 20 min at 0,65V<sub>Ag/AgCl</sub>, respectively.

The selected area was repeatedly scanned for 2 hours at OCP, but no topography change could be observed. Figure 4a shows an example of topography image after 2 hours at OCP. At all the applied potentials within the passive range (0.2 – 0.5 V<sub>Ag/AgCl</sub>), the surface morphology remained stable, without showing clear evidence of corrosion. At 0.65 V<sub>Ag/AgCl</sub> (Figure 4b), where the current already started to increase (current density 0,07 mA/cm<sup>2</sup>) the topography map recorded did not show any pronounced change compared to the previous images. Only a slight dissolution could be observed, starting at the matrix area nearby the carbide and from the defect itself. The results are consistent with the previous work [16-17], showing that the dissolution at the high anodic potential mainly takes place at phase and grain boundaries.

Instead of strong dissolution, a fast formation of oxygen bubbles could be seen by the camera placed on top of the AFM head, focused on the scanned and nearby areas (Figure 4 c-e, the red color is the AFM laser pointed onto the cantilever and scattered by the liquid surface). When the potential was held at 0.65 V<sub>Ag/AgCl</sub>, in few minutes many oxygen bubbles nucleated on the metal surface, grew for a time and then detached from the surface. The AFM measurements had to be stopped at the potential of

0.65 V<sub>Ag/AgCl</sub>, because it was not possible to maintain the contact between the tip and the sample surface, due to the large number of oxygen bubbles produced.

In aqueous electrolytes, oxidation of water can occur at sufficiently high potential on any metal surface, leading to formation of O<sub>2</sub> bubbles (Eq.8) [16].



Thermodynamically, water can be oxidized already at 0.6 V<sub>Ag/AgCl</sub>, which is the equilibrium potential at 25 °C, pH 7.4 [24]. The metal elements composing the sample (electrode) surface play an important role on the kinetics of this reaction. It is well known that cobalt is a good catalyst for electrochemical water oxidation [29-31]. It has been found that the catalytic influence of cobalt on water oxidation is further enhanced in presence of phosphate in neutral water under ambient conditions [29], through lowering the overpotential necessary to drive the reaction [30-31]. Furthermore, it has been verified that Co (II) species at the anode surface are oxidized to Co (III), and can catalyze the oxidation of water to intermediate peroxide species, which in turn spontaneously decompose to water and oxygen [29,32-33].

Catalytic oxidation of water to intermediate peroxide [32]:



Catalytic decomposition of peroxide by acid [32]:



A decrease in the overpotential needed for oxygen evolution generally indicates that the process is electrocatalyzed [32]. Rasiyah and Tseung [34] reported that there are oxides, including Co<sub>2</sub>O<sub>3</sub> and CoO<sub>2</sub>, on which intermediates are chemisorbed and oxygen bubbles evolve at low overpotential. Rüetschi and Delahay showed that the overpotential necessary for cobalt to catalyze the water oxidation is very little [33].

On the CoCrMo alloy, the surface oxide layer contains certain amount of cobalt oxides. Therefore, at a relatively low potential of ca. 0.7 V<sub>Ag/AgCl</sub>, water oxidation can occur and may become one of the important contributions to the total current recorded. As it can be observed from the in situ EC-AFM images shown in Figure 4a-b, no pronounced topography changes occurred at this potential, even in presence of a low amount of H<sub>2</sub>O<sub>2</sub>. Instead, the formation of oxygen bubbles at 0.65 V<sub>Ag/AgCl</sub> shown in Figure 4c-e is a clear evidence of the occurrence of oxygen evolution. As shown in Figure 4c-e, even with a very low concentration of H<sub>2</sub>O<sub>2</sub>, the formation of oxygen bubbles at 0.65 V<sub>Ag/AgCl</sub> was a fast process, enabling the visual observation by the camera. It should be emphasized that, the detected metal release is a result of anodic oxidation reactions at the applied potential at which the high current density is caused by the anodic polarization of the sample and water oxidation at the sample surface. Under real corrosion conditions (no polarization), the corrosion current density is a few orders of magnitude lower than this level.

#### 4. CONCLUSIONS

Combined electrochemical measurements, including cyclic potentiodynamic polarization, potentiostatic polarization, in-situ electrochemical AFM and LOM measurements, and metal release

analysis after the potentiostatic polarization at  $0.7 V_{Ag/AgCl}$  were performed to clarify the nature of the current increase at high anodic potential (over  $0.5 V_{Ag/AgCl}$ ) for a CoCrMo alloy exposed to PBS solution. The following conclusions can be drawn:

1. The cyclic potentiodynamic polarization curve showed the presence of a small positive loop, indicating some metal dissolution occurring at potentials above  $0.5 V_{Ag/AgCl}$ .
2. The potentiostatic polarization measurements and the metal release analyses of the solution confirmed the occurrence of some dissolution at  $0.7 V_{Ag/AgCl}$ , which corresponds to ca. 40% of the total current recorded at this potential. The three alloying elements were released nearly in proportion to their contents in the alloy.
3. In situ EC-AFM measurements of the alloy immersed in PBS + 3 mM  $H_2O_2$  did not show any pronounced topography change at the potential ( $0.65 V_{Ag/AgCl}$ ) where the current already started to increase. Instead, a fast nucleation and growth of oxygen bubbles on the sample surface was observed by the optical microscope focused on the scanned area.
4. It is clear that the increase of current recorded for the CoCrMo alloy at high anodic potential, over  $0.5 V_{Ag/AgCl}$ , is the sum of different contributions, and water oxidation is an important one.

#### ACKNOWLEDGEMENT

AB Sandvik Materials Technology, Sweden, is acknowledged for the financial support of this study and for supply of samples. Dr. Gunilla Herting, at the Div. of Surface & Corrosion Science at the Royal Institute of Technology (KTH), is acknowledged for the help with metal release analysis.

#### References

1. J. Reeman, A.M.I. Mech, R.W.A. Buswell, *Aircr. Eng. Aerosp. Tec.*, 25 (1953) 227
2. C.W. Foster, *Aircr. Eng. Aerosp. Tec.*, 55 (1983) 2
3. J.A. Disegi, R.L. Kennedy, R. Pilliar, *Cobalt-base alloys for biomedical applications*, VA: ASTM, Fredericksburg (1999)
4. Y. Liao, E. Hoffman, M. Wimmer, A. Fischer, J. Jacobs, L. Marks, *Phys. Chem. Chem. Phys.*, 15 (2013) 746
5. S. Kurz, A.W.E. Hodgson, S. Virtanen, V. Fervel, S. Mischler, *Eur. Cells Mater.*, 3 (2002) 26
6. R.W.-W. Hsu, C.-C. Yang, C.-A. Huang, Y.-S. Chen, *Mater. Chem. Phys.*, 93 (2005) 531
7. L. Casabán Julián, A. Igual Muñoz, *Tribol. Int.*, 44 (2011) 318
8. A. Igual Muñoz, S. Mischler, *J. Electrochem. Soc.*, 154 (2007) C562
9. A.W.E. Hodgson, S. Kurz, S. Virtanen, V. Fervel, C.-O.A. Olsson, S. Mischler, *Electrochim. Acta*, 49 (2004) 2167
10. C. Valero Vidal, A. Igual Muñoz, *Corros. Sci.*, 50 (2008) 1954
11. C. Valero Vidal, A. Igual Muñoz, *Electrochim. Acta*, 54 (2009) 1798
12. C. Valero Vidal, A. Igual Muñoz, *Electrochim. Acta*, 56 (2011) 8239
13. I. Milošev, H.-H. Strehblow, *Electrochim. Acta*, 48 (2003) 2767
14. Y.S. Li, K. Wang, P. He, B.X. Huang, P. Kovacs, *J. Raman Spectrosc.*, 30 (1999) 97
15. P. Schmuki, S. Virtanen, A. J. Davenport, C. M. Vitus, *J. Electrochem. Soc.*, 143 (1996) 3997
16. E. Bettini, T. Eriksson, M. Boström, C. Leygraf, J. Pan, *Electrochim. Acta*, 56 (2011) 9413
17. E. Bettini, C. Leygraf, C. Lin, P. Liu, J. Pan, *J. Electrochem. Soc.*, 159 (2012) C422
18. C. Valero Vidal, A. Igual Muñoz, *Electrochim. Acta*, 55 (2010) 8445

19. C. Valero Vidal, A. Igual Muñoz, C.-O.A. Olsson, S. Mischler, *J. Electrochem. Soc.*, 159 (2012) C233
20. B.E. Conway, *Comprehensive treatise of electrochemistry: kinetics and mechanisms of electrode processes*, Volume 7, Chapter 6, Plenum Press, New York (1983)
21. K. Midander, A. de Frutos, Y. Hedberg, G. Darrie, I. Odnevall Wallinder, *Integr. Environ. Assess. Manag.*, 6 (2009) 441
22. Y. Hedberg, K. Midander, I. Odnevall Wallinder, *Integr. Environ. Assess. Manag.*, 6 (2010) 456
23. M. Pourbaix, *Biomaterials*, 5 (1984) 122
24. M. Pourbaix, *Atlas of Electrochemical Equilibria in Aqueous solutions*, Pergamon Press, Oxford, (1996)
25. C. Leygraf, G. Hultquist, I. Olefjord, B.-O. Elfström, V.M. Knyazheva, A.V. Plaskeyev, Y.M. Kolotyркиn, *Corros. Sci.*, 19 (1979) 343
26. G. Herting, I. Odnevall Wallinder, C. Leygraf, *Corros. Sci.*, 49 (2007) 103
27. A. Seyeux, V. Maurice, P. Marcus, *Electrochem. Solid St.*, 12 (2009) C25
28. D.D. McDonald, *J. Electrochem. Soc.*, 139 (1992) 3434
29. M.W. Kanan, D.G. Nocera, *Science*, 321 (2008) 1072
30. D.K. Zhong, D.R. Gamelin, *J. Am. Chem. Soc.*, 132 (2010) 4202
31. M. Musiani, *Chem. Commun.*, 21 (1996) 2403
32. A.N. Nikoloski, M.J. Nicol, *Mineral Processing & Extractive Metall. Rev.*, 31 (2010) 30
33. P. Ruetschi, P. Delahay, *J. Chem. Phys.*, 23 (1955) 556
34. P. Rasiyah, A.C.C. Tseung, *J. Electrochem. Soc.*, 131 (1984) 803